Competitive autocatalytic reactions in chaotic flows with diffusion: Prediction using finite-time Lyapunov exponents

Conor P. Schlick, Paul B. Umbanhowar, Julio M. Ottino, and Richard M. Lueptow

Citation: Chaos: An Interdisciplinary Journal of Nonlinear Science **24**, 013109 (2014); doi: 10.1063/1.4862153
View online: http://dx.doi.org/10.1063/1.4862153
View Table of Contents: http://scitation.aip.org/content/aip/journal/chaos/24/1?ver=pdfcov
Published by the AIP Publishing

Competitive autocatalytic reactions in chaotic flows with diffusion: Prediction using finite-time Lyapunov exponents

Conor P. Schlick,[1,a)] Paul B. Umbanhowar,[2] Julio M. Ottino,[2,3,4] and Richard M. Lueptow[2,4,b)]
[1]*Department of Engineering Sciences and Applied Mathematics, Northwestern University, Evanston, Illinois 60208, USA*
[2]*Department of Mechanical Engineering, Northwestern University, Evanston, Illinois 60208, USA*
[3]*Department of Chemical and Biological Engineering, Northwestern University, Evanston, Illinois 60208, USA*
[4]*The Northwestern Institute on Complex Systems (NICO), Northwestern University, Evanston, Illinois 60208, USA*

(Received 30 September 2013; accepted 2 January 2014; published online 21 January 2014)

We investigate chaotic advection and diffusion in autocatalytic reactions for time-periodic sine flow computationally using a mapping method with operator splitting. We specifically consider three different autocatalytic reaction schemes: a single autocatalytic reaction, competitive autocatalytic reactions, which can provide insight into problems of chiral symmetry breaking and homochirality, and competitive autocatalytic reactions with recycling. In competitive autocatalytic reactions, species B and C both undergo an autocatalytic reaction with species A such that $A + B \rightarrow 2B$ and $A + C \rightarrow 2C$. Small amounts of initially spatially localized B and C and a large amount of spatially homogeneous A are advected by the velocity field, diffuse, and react until A is completely consumed and only B and C remain. We find that local finite-time Lyapunov exponents (FTLEs) can accurately predict the final average concentrations of B and C after the reaction completes. The species that starts in the region with the larger FTLE has, with high probability, the larger average concentration at the end of the reaction. If B and C start in regions with similar FTLEs, their average concentrations at the end of the reaction will also be similar. When a recycling reaction is added, the system evolves towards a single species state, with the FTLE often being useful in predicting which species fills the entire domain and which is depleted. The FTLE approach is also demonstrated for competitive autocatalytic reactions in journal bearing flow, an experimentally realizable flow that generates chaotic dynamics. © *2014 AIP Publishing LLC*. [http://dx.doi.org/10.1063/1.4862153]

In many physical systems where chemical reactions occur, the chemicals are also moved in space by the action of velocity fields (e.g., currents in the ocean or the atmosphere) and by molecular diffusion. We have developed a computational method that accurately and efficiently simulates these reacting, flowing, and diffusing systems—a task which in general is quite difficult. Our method allows us to quickly perform many simulations and thereby statistically study the chemical state of the system after the reaction is complete. We find that the degree of small scale stretching of the fluid elements at the initial spatial positions of the reactants that occurs early in the flow can accurately predict the final chemistry.

I. INTRODUCTION

In advection-reaction-diffusion (ARD) systems, chemical species simultaneously are advected by a velocity field, diffuse, and undergo a chemical reaction. ARD systems are relevant to many natural systems, for example, plankton populations[1,2] and ozone depletion in the Arctic,[3] as well as to engineering applications such as polymer processing[4] and micromixers.[5] ARD systems with nonlinear chemical reactions have been previously used to study the fingering dynamics of reaction-diffusion acidity fronts in the chlorite-tetrathionate reaction,[6] Marangoni convection patterns driven by a neutralization reaction,[7] and barriers to front propagation in the Belousov-Zhabotinsky reaction (i.e., "burning invariant manifolds").[8–11] In ARD systems, the underlying velocity field is critical in determining final species concentrations. By analyzing the velocity field using techniques from dynamical systems theory, specifically the finite-time Lyapunov exponent, we are able to accurately predict the average final species concentrations from the initial conditions in spite of the complex dynamics that often take place within ARD systems.

To study the relation of the finite-time Lyapunov exponent on ARD systems, we consider autocatalytic reactions where species B is autocatalyzed by species A

$$A + B \rightarrow 2B. \qquad \text{(R1)}$$

One notable example of autocatalytic reactions in ARD systems is the asymmetry in the autocatalysis of $NaClO_3$ crystals with a particular chirality.[12] In crystallization, a "mother crystal" of either type (levo- or dextro-rotatory) generates

a)Electronic mail: conorschlick2015@u.northwestern.edu
b)Electronic mail: r-lueptow@northwestern.edu

secondary crystals of the same chirality through autocatalytic secondary nucleation, a nonlinear process.[13] Experiments[14] in crystallization of $NaClO_3$ show that, if the crystallization occurs in an unstirred fluid, equal numbers of levo- and dextro-rotatory crystals are produced, and the mixture is said to be racemic. However, if stirred, there is typically a great disparity in the number of levo- and dextro-rotatory crystals, which is called a homochiral mixture, implying that chaotic advection plays a critical role in this form of crystallization.[12] Additional experimental studies have observed homochirality in the autocatalysis of chiral pyrimidyl alkanol,[15] and of various inorganic[16] and organic[17–19] molecules via chaotic advection and grinding, where glass beads grind larger crystals into smaller pieces which can be dissolved in solution. Homochirality can be useful in many applications. For instance, in pharmaceuticals, molecules of different chirality can have different properties, and only one may be desirable.[20]

Motivated by the $NaClO_3$ symmetry breaking experiments,[14] Metcalfe and Ottino[21] studied competitive autocatalytic reactions within a Lagrangian framework. In a competitive autocatalytic reaction, two species, B and C, undergo an autocatalytic reaction with species A

$$\begin{aligned} A + B &\rightarrow 2B, \\ A + C &\rightarrow 2C. \end{aligned} \tag{R2}$$

Initially, one B and one C particle are placed in a domain with many A particles, and all the particles are advected by a velocity field. If an A particle gets "close enough" to a B/C particle, it turns into a B/C particle. In their simulations, a large inequality in the final number of B and C particles is observed after all the A particles are consumed,[21] analogous to the homochiral state observed in experiments.[14] Moreover, differences in the initial location of the reacting particles in relation to the unstable manifold of a hyperbolic point gave drastically different results for the final relative numbers of B and C particles.

Several other computational and analytic studies have attempted to model homochirality. The earliest model is from Frank,[22] who added a recycling reaction to the two competitive autocatalytic reactions: $B + C \rightarrow 0$. In the absence of chaotic advection and diffusion, this set of reactions yields a homochiral state. To better understand homochirality, more recent modifications to Frank's model have incorporated spontaneous generation of B and C particles from achiral reactants (primary nucleation),[23,24] higher order autocatalytic reactions,[25] Ostwald ripening,[20,26,27] and grinding.[27,28] Other studies have stochastically considered homochirality to determine the final probability distribution of levo- or dextro-rotatory crystals.[29–31]

There are still several questions associated with our understanding of autocatalytic reactions in ARD systems. First, many numerical simulations approach this problem from a Lagrangian framework in the limit of infinitely fast reactions, an assumption that makes it difficult to study autocatalytic reactions across a broad range of physical parameters, including dependence on the diffusion coefficient and the reaction rate. Second, several studies[26–28] simulate chaotic advection by randomly redistributing the particles, which ignores the importance of the chaotic velocity field. Finally, there is not yet a predictive model for the dependence of the final average concentrations on the initial spatial conditions.

Previous studies have considered autocatalytic reactions in terms of global properties of the flow. Muzzio and Liu[32] showed that reactions occur more quickly for fully chaotic flows as compared to partially chaotic or regular flows. More recently, it has been shown that, depending on the parameters, the reaction speed (i.e., how quickly the average concentration of the reactants decreases) can depend on the Lyapunov exponent,[33,34] the spatial distribution of the finite-time Lyapunov exponent,[35] the dynamics of an effective fractal dimension,[34,36] and an effective diffusivity.[35] While the decay rate of the reactants can be quantified in terms of global properties of the flow, there has not yet been an approach to explain the dependence of the reaction speed on the initial conditions, and these ideas have not been extended to competitive autocatalytic reactions.

In this paper, we first present an accurate and efficient numerical method for solving ARD systems that enables a large number of simulations with different physical parameters to be investigated in a relatively short amount of time. Using this method, we show how the time for the reaction to complete and the final average concentrations vary depending on initial spatial conditions and the physical parameters of the problem. Finally, we present and develop a relatively simple approach that predicts final average concentrations using only the finite-time Lyapunov exponent at the initial placements of B and C, despite the complex dynamics associated with competitive autocatalytic reactions in the ARD system we examine.

II. METHODS

Successful modeling of autocatalytic reaction (R1) in ARD systems can, in general, be difficult, so infinitely fast (or diffusion limited) reactions[37] are often considered to simplify the modeling. In this limit, reactions only occur at the interface between A and B, and therefore, from an Eulerian viewpoint, each species has a concentration of 0 or 1 everywhere. When slow diffusion occurs at this interface, A is consumed by B, thus advancing the interface towards A. The infinitely fast reaction limit, described in detail elsewhere,[38] has been used to study autocatalytic reactions in relation to the unstable manifold of a hyperbolic fixed point,[39,40] fractal dimension and escape rate in an open flow,[41,42] and barriers to front propagation.[8–10] From an Eulerian point of view, the infinitely fast reaction limit requires the tracking of material lines in a chaotic flow, which is a difficult numerical problem.[43] For this reason, it is convenient to consider the infinitely fast reaction limit from a Lagrangian point of view. While convenient numerically, the Lagrangian framework has several shortcomings in ARD systems. First, Lagrangian methods have several artificial numerical parameters, such as the density of particles in the domain and a length scale related to how close

the particles must be to react. While these quantities relate to the physical parameters of the problem (e.g., the reaction rate and the diffusion coefficient), the precise mathematical relation is unclear. Second, the infinitely fast reaction limit, while appropriate for some applications, cannot capture reactions where the reaction timescale is comparable to or longer than the diffusion or advection timescales. In ARD systems in general, the concentrations of A and B vary continuously from 0 to 1 throughout the domain, and the infinitely fast reaction limit is not valid.

It is therefore useful to consider the full ARD problem from an Eulerian viewpoint. ARD systems have been previously solved using finite differences[32] and Galerkin spectral methods.[35,44–46] In this paper, we solve the ARD equation using an Eulerian framework by generalizing an operator splitting method. This method is accurate and has relatively low computational cost, allowing a large number of simulations to be performed over a wide range of physical parameters in a relatively short time. Operator splitting schemes for advection-diffusion problems, which have been verified to be accurate,[47] have been used to study magnetic field diffusion in fast dynamos,[48] tracer trajectories in turbulent flows,[49] and strange eigenmodes in granular flows.[50] In reacting flows, many Lagrangian studies implement operator splitting techniques as well (i.e., particles advect for some time, then instantaneously react),[39–42,51,52] but these studies are subject to the limitations of the Lagrangian approach mentioned above.

A. Eulerian advection-reaction-diffusion

The non-dimensional ARD equation for species i is[51]

$$\frac{\partial c_i}{\partial t} + \boldsymbol{u}\cdot\nabla c_i = \frac{1}{\mathrm{Pe}}\nabla^2 c_i + \mathrm{Da}R_i(c_A, c_B, c_C), \tag{1}$$

where $c_i(\boldsymbol{x},t)$ is the concentration of species i (i.e., $i=A$, $i=B$, or $i=C$), $\boldsymbol{u}$ is the advective velocity field, and R_i is a rate function that characterizes the chemical reaction. The Péclet number is $\mathrm{Pe} = UL/D$ and the Damköhler number is $\mathrm{Da} = kL/U$, where L is a characteristic length, U is a characteristic velocity, D is the diffusion coefficient, and k is a reaction rate. Physically, Pe represents the ratio of an advection rate to a diffusion rate, and Da represents the ratio of a reaction rate to an advection rate. If the velocity field is incompressible ($\nabla\cdot\boldsymbol{u}=0$), each species has the same diffusion coefficient,[53] and $\sum_i R_i = 0$, then the total species concentration is conserved, i.e., if $\sum_i c_i(\boldsymbol{x}, t=0) = 1$ for all $\boldsymbol{x}$, then $\sum_i c_i(\boldsymbol{x},t) = 1$ for all $\boldsymbol{x}$ and $t>0$. For the autocatalytic reaction in reaction scheme (R1),

$$R_B(c_A, c_B) = -R_A(c_A, c_B) = c_A c_B. \tag{2}$$

The advective velocity field we consider here is time-periodic sine flow (TPSF),[54,55] a two-dimensional flow used in several other ARD studies.[1,32,44,56] The velocity field of TPSF (shown schematically in Figs. 1(a) and 1(b)), which is defined on the unit square ($0\le x, y\le 1$) with periodic boundary conditions, is

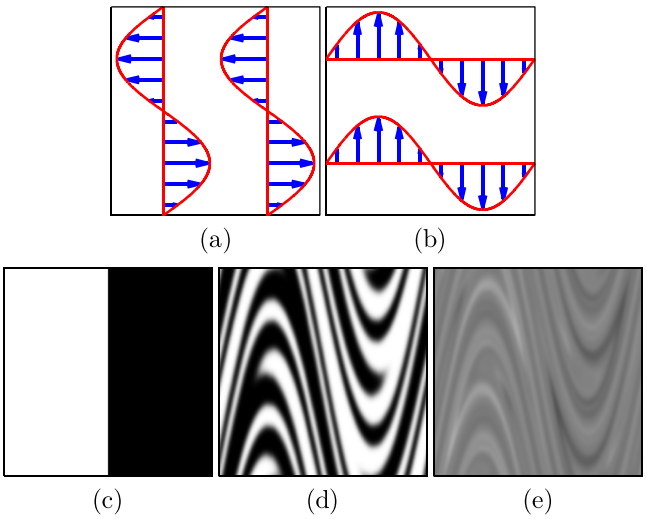

FIG. 1. Schematic of the velocity field of TPSF for (a) $0 \le \mathrm{mod}\,(t,T) < T/2$ and (b) $T/2 \le \mathrm{mod}\,(t,T) < T$. Concentration distributions for TPSF of a single species under advection-diffusion with $\mathrm{Pe} = 10^4$ (c) for the initial condition, (d) after 1 period, and (e) after 4 periods. $0 \le x, y \le 1$, where x is the abscissa and y is the ordinate.

$$\boldsymbol{u}(x,y,t) = \begin{cases} \sin(2\pi y)\hat{\boldsymbol{x}}, & 0 \le \mathrm{mod}\,(t,T) < T/2, \\ \sin(2\pi x)\hat{\boldsymbol{y}}, & T/2 \le \mathrm{mod}\,(t,T) < T. \end{cases} \tag{3}$$

The period of the flow, T, is free to be chosen, and different values for T can give a partially chaotic flow (visible islands of regular flow) or a fully chaotic flow (no visible islands).[57] We use $T = 1.6$, which makes the velocity field fully chaotic in the entire domain. Concentration distributions for advection-diffusion (Eq. (1) with $\mathrm{Pe} = 10^4$ and $\mathrm{Da} = 0$) under TPSF are shown in Figs. 1(c)–1(e) for a segregated initial condition ($c=1$ for $x<0.5$ and $c=0$ for $x>0.5$). The concentration distributions show that TPSF is fully chaotic with substantial blurring of striations due to diffusion at $t = 4T$ for $T = 1.6$.

B. Numerical method

Similar to the approach in Schlick *et al.*,[47] to evolve the system from time $t = m\Delta t$ to $t = (m+1)\Delta t$, we first solve the advection step

$$\frac{\partial c_i^*}{\partial t} = -\boldsymbol{u}\cdot\nabla c_i^*, \quad t\in[m\Delta t, (m+1)\Delta t], \tag{4}$$

for $c_i^*((m+1)\Delta t)$ using $c_i(m\Delta t)$ as the initial condition. Next, the diffusion step is solved,

$$\frac{\partial c_i^{**}}{\partial t} = \frac{1}{Pe}\nabla^2 c_i^{**}, \quad t\in[m\Delta t, (m+1)\Delta t], \tag{5}$$

for $c_i^{**}((m+1)\Delta t)$ using $c_i^*((m+1)\Delta t)$ as the initial condition. Finally, the reaction step is solved

$$\frac{\partial c_i}{\partial t} = \mathrm{Da}R_i(c_A, c_B, c_C), \quad t\in[m\Delta t, (m+1)\Delta t], \tag{6}$$

for $c_i((m+1)\Delta t)$ using $c_i^{**}((m+1)\Delta t)$ as the initial condition.

To solve each step, the domain is subdivided into an N_x by N_y grid (with $N_x = N_y = 300$). The advection step (Eq. (4)) is solved with a matrix mapping method.[47,50,58,59] The matrix mapping method uses an $N_xN_y \times N_xN_y$ matrix, $\mathbf{\Phi}_{t_0,\Delta t}$, where each entry $\mathbf{\Phi}_{t_0,\Delta t}^{(j_1,j_2)}$ is the proportion of material in cell j_1 carried by the velocity field $\boldsymbol{u}$ from cell j_2 from time t_0 to time $t_0 + \Delta t$. Letting $\boldsymbol{c}_i$ be an $N_xN_y \times 1$ column vector of the concentrations in each grid cell, then $\boldsymbol{c}_i^*(t_0 + \Delta t) = \mathbf{\Phi}_{t_0,\Delta t}\boldsymbol{c}_i^*(t_0)$. To solve the diffusion step, a backward Euler scheme is implemented as in Marchuk–Yanenko operator splitting.[60] To solve the reaction step, a 4th order Runge-Kutta scheme is used in each grid cell.

C. Finite-time Lyapunov exponent

To characterize the local dynamics of the flow field, we use the finite-time Lyapunov exponent (FTLE). Following Shadden *et al.*,[61] consider the differential equation

$$\frac{d\boldsymbol{x}}{dt} = \boldsymbol{u}(\boldsymbol{x}, t), \tag{7}$$

which describes the Lagrangian motion of a particle under a velocity field $\boldsymbol{u}$. If a tracer is started at an initial location $\boldsymbol{x}$ at $t = t_0$, let $\phi_{t_0,\tau}(\boldsymbol{x})$ be the location of the tracer after time τ. The finite-time right Cauchy-Green deformation tensor is then given as

$$\Delta^{(t_0,\tau)}(\boldsymbol{x}) = \frac{d\phi_{t_0,\tau}(\boldsymbol{x})^*}{d\boldsymbol{x}}\frac{d\phi_{t_0,\tau}(\boldsymbol{x})}{d\boldsymbol{x}}, \tag{8}$$

where the * indicates the complex conjugate. From here, the finite-time Lyapunov exponent is

$$\lambda^{(t_0,\tau)}(\boldsymbol{x}) = \frac{1}{|\tau|}\log\sqrt{\Lambda_{\max}\left(\Delta^{(t_0,\tau)}(\boldsymbol{x})\right)}, \tag{9}$$

where $\Lambda_{\max}(\Delta)$ is the largest eigenvalue of Δ. Thus, the FTLE represents the maximum separation of two nearby points over a finite interval of time. For the rest of this paper, we take $t_0 = 0$, so $\lambda^{(\tau)}(\boldsymbol{x}) \equiv \lambda^{(t_0,\tau)}(\boldsymbol{x})$. In this definition, τ can be either positive or negative, and taking $\tau \to \infty$ gives the typical definition of the (infinite-time) Lyapunov exponent.

Figure 2 shows the FTLE for TPSF for different values of τ. For $\tau = T/2$, the flow is independent of x, so the FTLE is also independent of x. As τ increases, a more complex structure emerges: since the velocity field is chaotic, initially nearby points move away from each other and can undergo very different dynamics as time progresses.

III. AUTOCATALYTIC REACTIONS

A. Autocatalytic reaction with one species

Consider a single autocatalytic reaction (R1) (with R_i given by Eq. (2)). Initially, the concentration of B, c_B, is 0 everywhere except in one grid cell, where $c_B = 1$. The rest of the domain is filled with species A by setting $c_A = 1$. Thus, $c_A + c_B = 1$ everywhere in the domain. Let $\lambda_B^{(\tau)}$ be the finite-time Lyapunov exponent at the center of the single starting grid cell for B.

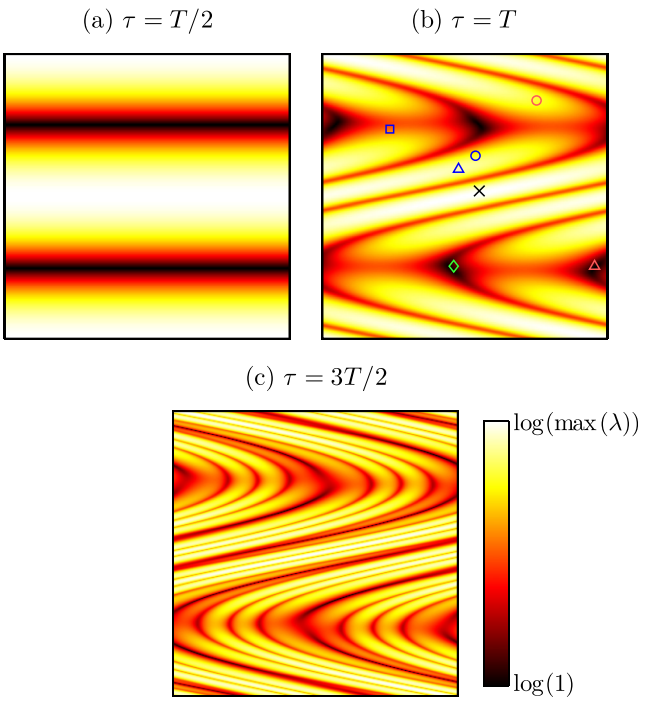

FIG. 2. FTLE for TPSF for various τ on a log scale. In (b), the symbols indicate the initial conditions for Figures 3–5. The maximum values of λ (white) are (a) $\max(\lambda) = 27.22$, (b) $\max(\lambda) = 741.4$, and (c) $\max(\lambda) = 2018$.

Figure 3 shows an example of the evolution of c_A and c_B based on Eq. (1) for an autocatalytic reaction (R1) where B is initially placed in the region indicated by the square symbol in Figure 2(b). In Figure 3, white represents species A and black (blue online) represents species B. For short times ($t = T/2$), B remains localized. However, as time evolves, B stretches, diffuses, and reacts, until it nearly fills the entire domain at $t = 5T/2$. For intermediate times, species B aligns with the unstable manifold of a hyperbolic fixed point in the

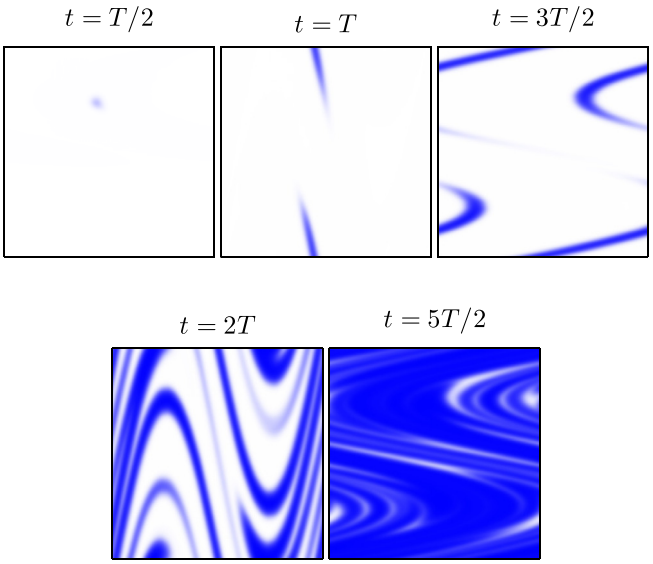

FIG. 3. Concentration distributions of ARD for an autocatalytic reaction (R1) under TPSF. A (white) and B (black, blue online). $\lambda_B^{(T)} = 33.61$, $\mathrm{Pe} = 10^4$, $\mathrm{Da} = 5$. Starting location of B in relation to the FTLE for $\tau = T$ is indicated by the square symbol in Figure 2(b).

flow, causing the unstable manifold to appear "fattened," as reported in previous studies.[39,40]

Figure 4(a) shows the average concentration of A as a function of time for three different initial placements of B in the domain. In each case, there is a long transient where $\langle c_A \rangle \approx 1$, after which $\langle c_A \rangle$ decreases exponentially, which is consistent with earlier studies.[34–36] For the three different initial conditions, $\langle c_A \rangle$ decays at the same rate after the transient; however, the length of the transient varies with the initial conditions. For $\lambda_B^{(T)}$ small, the transient is longer, as there is less initial stretching of B, and B spreads more slowly throughout the domain. For $\lambda_B^{(T)}$ large, B stretches significantly initially, and spreads out more quickly; thus the transient is shorter. Despite a difference of almost three orders of magnitude in $\lambda_B^{(T)}$, the time to achieve $\langle c_A \rangle = 10^{-3}$ only differs by about $\pm 10\%$. While the FTLE does not significantly influence single autocatalytic reactions, Sec. III B shows that the FTLE is immensely important for competitive autocatalytic reactions, since a small initial bias in one of the species is greatly amplified.

To demonstrate the effect of different Péclet and Damköhler numbers, Fig. 4(b) shows the reaction time as a function of Da for three different values of Pe. We define the reaction time, t_r, as the time (averaged over 50 randomly chosen initial placements of B) for the average concentration of A to be reduced to 10^{-3}. The reaction time decreases as Da increases, with the fastest reaction occurring for the lowest Pe, as expected. For Da small (reaction-limited), there is little difference in t_r for different Pe (2% difference between $\mathrm{Pe} = 10^3$ and $\mathrm{Pe} = 10^5$ for $\mathrm{Da} = 1$). In this regime of slow reactions, B spreads (due to chaotic advection and diffusion) through the entire domain more quickly than the reaction can occur, so the reaction takes approximately the same time to complete regardless of Pe.

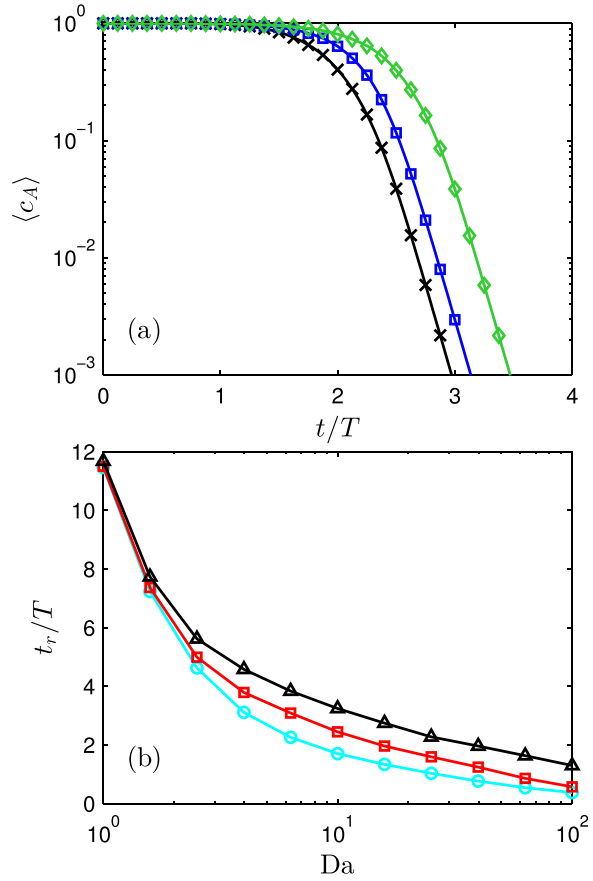

FIG. 4. (a) Average concentration of A vs. time for different initial placements of B: $\lambda_B^{(T)} = 689.7$ (×), $\lambda_B^{(T)} = 33.61$ (□), and $\lambda_B^{(T)} = 1.667$ (◇). Starting locations for B are indicated in Figure 2(b) (by corresponding symbols). Spatial concentration distributions at various times for $\lambda_B^{(T)} = 33.61$ (□) are shown in Figure 3. $\mathrm{Pe} = 10^4$ and $\mathrm{Da} = 5$. (b) Average time for reaction to complete vs. Da for $\mathrm{Pe} = 10^3$ (○), $\mathrm{Pe} = 10^4$ (□), and $\mathrm{Pe} = 10^5$ (△).

B. Competitive autocatalytic reaction

Consider now competitive autocatalytic reactions (R2) in which B and C compete for A, and the system is evolved until species A is exhausted. In this reaction, the reaction functions R_i from Eq. (1) are

$$\begin{aligned} R_B &= c_A c_B, \\ R_C &= c_A c_C, \\ R_A &= -c_A c_B - c_A c_C. \end{aligned} \tag{10}$$

This reaction scheme was previously studied by Metcalfe and Ottino[21] and was motivated by $NaClO_3$ symmetry breaking experiments.[14] In simulations, initially both B and C are localized to single, distinct grid cells, and the rest of the domain is composed of A, so $c_A + c_B + c_C = 1$ everywhere in the domain. We define the ratio of the finite-time Lyapunov exponents at the starting locations of B and C as

$$L^{(\tau)} = \lambda_B^{(\tau)} / \lambda_C^{(\tau)}. \tag{11}$$

After a simulation has completed, $\langle c_A \rangle = 0$, and the spatially averaged final concentrations of B and C, $c_B^\infty \equiv \langle c_B(t=\infty) \rangle$ and $c_C^\infty \equiv \langle c_C(t=\infty) \rangle$, are calculated.[62] Note that $c_B^\infty + c_C^\infty = 1$, since $\langle c_A \rangle + \langle c_B \rangle + \langle c_C \rangle = 1$ for all t. The ratio of the final concentrations, defined as $c^\infty = c_B^\infty / c_C^\infty$, indicates the relative final concentrations of B and C.

Figure 5 shows the evolution of A (white), B (black, blue online), and C (grey, red online) for two sample simulations with different initial conditions, and Figure 6 shows the average concentration of the three species as a function of time. The initial placements of B and C are indicated on Figure 2(b) to show their relation to the FTLE for $\tau = T$. In the first simulation (S1), $L^{(T)} \approx 1$ and $c^\infty \approx 1$, meaning both B and C end up covering about the same area in the domain in the long run (see $t = 5T/2$ for S1 in Figure 5). In this case, both B and C undergo approximately the same amount of initial stretching in the flow, as indicated by similar values for the FTLE at their initial location and as evident in S1 in Figure 5 at $t = T$. However, in the second simulation (S2), $L^{(T)} \gg 1$, indicating that B is initially stretched more than C. This is evident for $t = T/2$ and $t = T$ for S2 in Figure 5, where B has stretched significantly ($\lambda_B^{(T)}$ is large), while C has been stretched very little ($\lambda_C^{(T)}$ is small). This asymmetry in the stretching creates a small initial bias (which can be seen for $t \approx T$ in Figure 6(b)) that is amplified as time goes on, as described in Bonner[63,64] and observed in experiments.[15] The final result is that B dominates C, as is evident

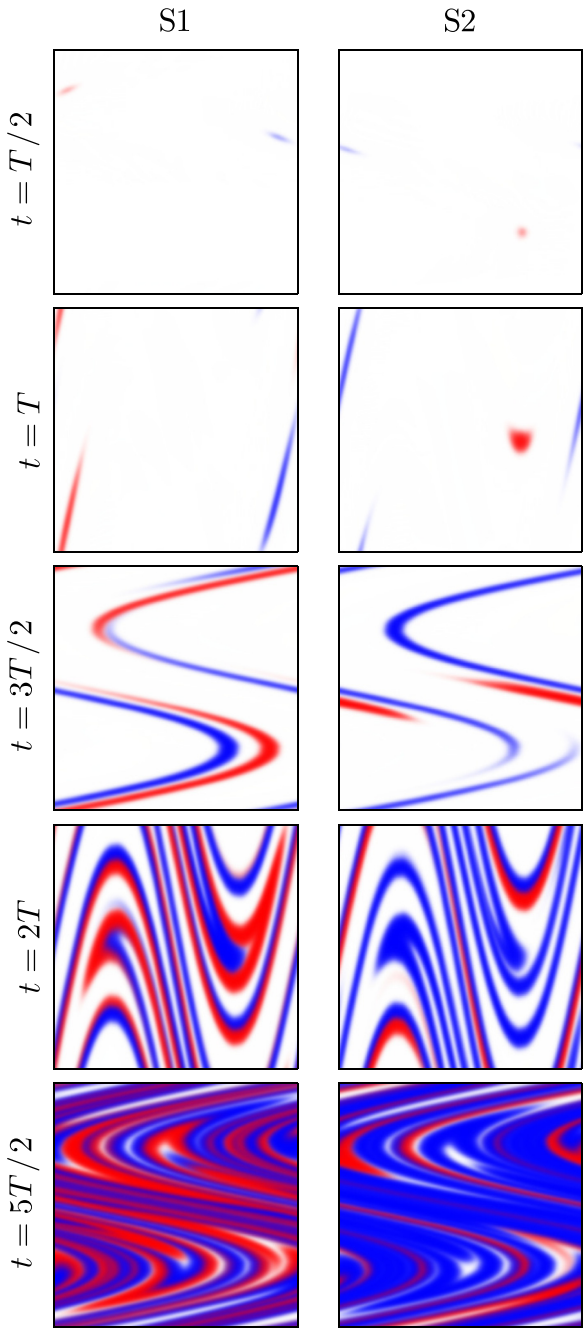

FIG. 5. Concentration distributions of ARD for a competitive autocatalytic reaction (R2) under TPSF. A (white), B (black, blue online), and C (grey, red online). (S1) $L^{(T)} = 193.0/194.5 = 0.99$ and $c^{\infty} = 0.539/0.461 = 1.17$. (S2) $L^{(T)} = 425.3/1.03 = 412.9$ and $c^{\infty} = 0.822/0.178 = 4.62$. $\mathrm{Pe} = 10^4$ and $\mathrm{Da} = 5$. Initial placements of B and C are shown in relation to the FTLE for $\tau = T$ in Figure 2(b) for S1 (○) and S2 (△).

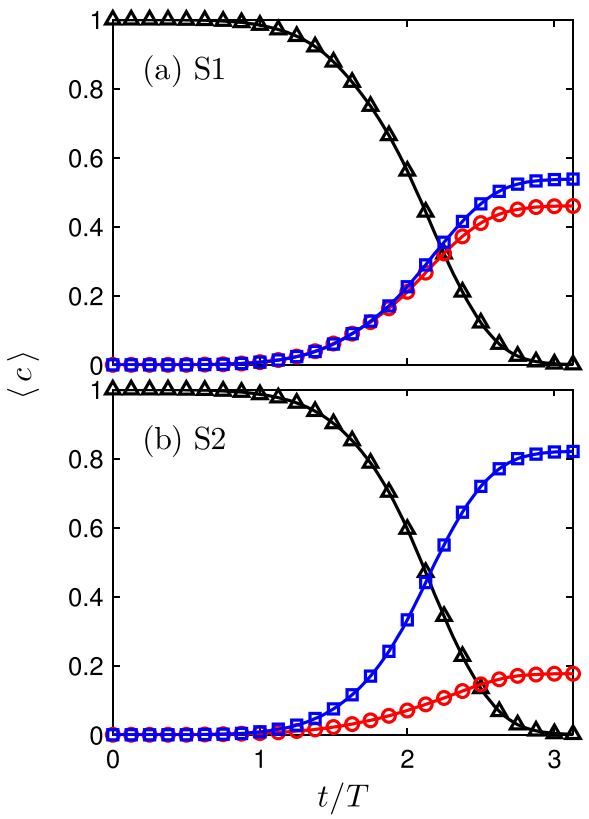

FIG. 6. Average concentrations of A (△), B (□), and C (○) vs. time for the simulations shown in Figure 5.

for $t = 5T/2$ for S2 in Figure 5, and $c^{\infty} \approx 5$, indicating that B ends up covering nearly five times more of the domain than C, as seen for later times in Figure 6.

To capture the range of final possible configurations, Figure 7 shows histograms of different outcomes (c_B^{∞}) for different Péclet and Damköhler numbers. Each histogram includes 1000 trials, and in each trial, the initial placements of B and C are randomly chosen. Panels (a)–(c) show the effect of the Damköhler number on c_B^{∞} with constant $\mathrm{Pe} = 10^4$. For Da small (Figure 7(a)), there is little spread in the data ($0.37 < c_B^{\infty} < 0.63$), as the reaction occurs so slowly that both species spread across most of the domain due to diffusion and chaotic advection before they react much. Consequently, both species are approximately equally spread throughout the domain after the reactions complete. For Da large (Figure 7(c)), the reaction occurs quickly, and the initial concentrations of B and C grow rapidly, not allowing time for stretching. This nullifies the effects of chaotic advection and again produces a state with approximately equal average concentrations of B and C. However, for intermediate values of Da ($2 < \mathrm{Da} < 20$), the reaction is neither too slow nor too fast. Consequently, the initial stretching of fluid elements plays an important role in determining the final state.

In Figures 7(d)–7(f) ($\mathrm{Da} = 5$, varying Pe), it is evident that increasing Pe broadens the histogram. For smaller Pe, B and C diffuse more quickly, reducing the importance of chaotic advection at the specific initial placements of reactants and resulting more frequently in states with $c_B^{\infty} \approx 0.5$. For $\mathrm{Pe} < 10^3$, the histogram would continue to narrow, since both species will spread equally throughout the domain before they react much, similar to panel (a). As Pe increases, the efficacy of diffusion decreases, and the small scale interactions of fluid elements by chaotic advection become more important. Therefore, as in simulation S2 in Figure 5, either B or C can be stretched more initially. As a result, it is more likely that a large disparity in the final concentrations occurs by the end of the reaction.

To quantitatively determine the effect of the finite-time Lyapunov exponent on final average concentrations, Figure 8

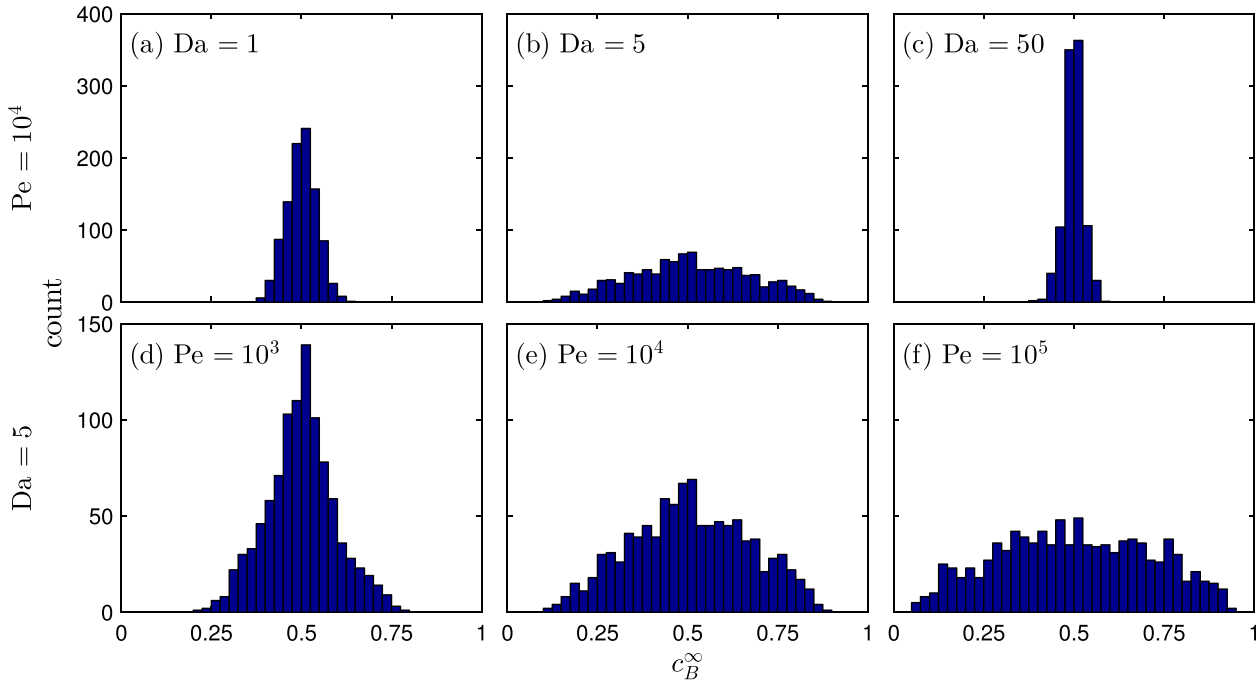

FIG. 7. Histograms of c_B^∞ for 1000 trials of ARD for competitive autocatalytic reactions (R2) under TPSF with various values of Pe and Da. Note that panels (b) and (e) both correspond to $\mathrm{Pe} = 10^4$ and $\mathrm{Da} = 5$ with different vertical scales.

shows scatter plots of c^∞ as a function of $L^{(\tau)}$. When $L^{(\tau)} \approx 1$ (B and C start at locations of approximately equal FTLE), a state with nearly equal average concentrations of B and C is typically formed and $c^\infty \approx 1$. When $L^{(\tau)} > 1$, B is stretched more initially and $c_B^\infty > c_C^\infty$ ($c^\infty > 1$). Similarly, when $L^{(\tau)} < 1$, C is initially stretched more than B and $c^\infty < 1$. The relationship can be approximated as

$$c^\infty = \left(L^{(\tau)}\right)^\gamma, \tag{12}$$

where γ can be determined by fitting the data in Figure 8 to a line. This simple relation connects the small scale stretching (given by the FTLE) to the averaged long term behavior of the system, dramatically simplifying the complex dynamics associated with the solution to the ARD equation (1). Similar results were obtained for $10^3 < \mathrm{Pe} < 10^5$ and $2 < \mathrm{Da} < 20$, since these values result in a wider spread for c^∞ (see Figure 7). Outside these ranges, histograms of c_B^∞ are narrow (like Figures 7(a) and 7(c)) as chaotic advection is less important,

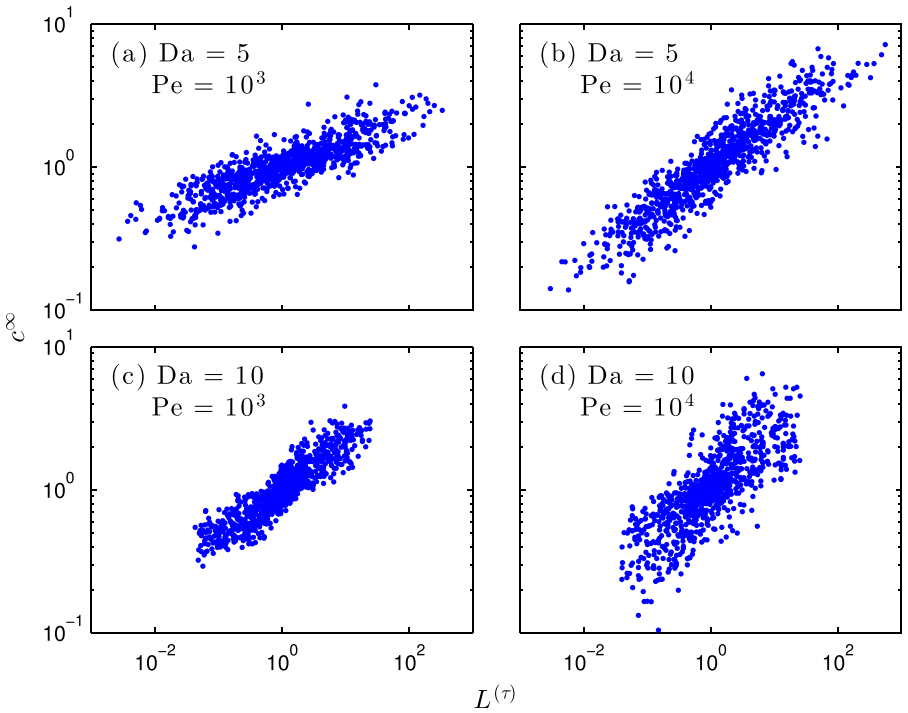

FIG. 8. Effect of the FTLE ratio $L^{(\tau)}$ on the concentration ratio c^∞ for TPSF for $\mathrm{Da} = 5$, 10 and $\mathrm{Pe} = 10^3$, 10^4. (a) $\tau = T$, $\gamma = 0.168$. (b) $\tau = T$, $\gamma = 0.330$. (c) $\tau = T/2$, $\gamma = 0.326$. (d) $\tau = T/2$, $\gamma = 0.371$. Each data set (for each pair of parameters) includes 1000 trials with different randomly chosen initial placements of B and C.

and Eq. (12) does not effectively describe the reaction dynamics.

The results shown in Figure 8 are weakly dependent on τ. In general, choosing $\tau = T/2$, T, or $3T/2$ is sufficient to achieve good results (i.e., high R^2 value of the fit of a line to the data in Figure 8) in the given parameter range ($10^3 < \mathrm{Pe} < 10^5$ and $2 < \mathrm{Da} < 20$). The values for τ used in Figure 8 are chosen by calculating the largest R^2 value (for $\tau = T/2$, T, or $3T/2$) of the fit of equation (12) to the data in Figure 8. The optimal value for τ is related to how long it takes to complete the reaction (see Figure 4(b)). For example, when $\mathrm{Da} = 5$ (Figures 8(a) and 8(b)), the reaction takes longer to complete than when $\mathrm{Da} = 10$. Thus, the τ used for $\mathrm{Da} = 5$ is larger than that used for $\mathrm{Da} = 10$. The parameter γ, which is obtained by fitting the data to a power law, is related to the range of the data in Figure 7. In Figure 7(d), the range for c_B^∞ is narrower than in Figure 7(e), so for $\mathrm{Da} = 5$, the value for γ for $\mathrm{Pe} = 10^3$ is smaller than the value for γ for Pe 10^4.

From the results in Figure 8, it is possible to predict the histogram of final concentration distributions (Figure 7) from the FTLE distribution. From Eq. (12) and noting that $c^\infty = c_B^\infty / c_C^\infty = c_B^\infty / (1 - c_B^\infty)$, we obtain the relation

$$c_B^\infty = \frac{1}{1 + \left(L^{(\tau)}\right)^{-\gamma}}. \tag{13}$$

To obtain a probability density function for $L^{(\tau)}$, 10^6 pairs of points were randomly chosen, and the ratio of the FTLE at those points was calculated. The results for the predicted probability density function from the FTLE distribution (using Eq. (13)) are compared to the actual probability density function obtained from numerical simulations of the ARD equation (1) in Figure 9. Indeed, the predicted distribution matches the simulations. While it is necessary to know τ and γ to predict the histogram, these can be obtained from relatively few simulations. The probability density function can then be extrapolated from the FTLE distribution using Eq. (13), which is generally less computationally expensive than running many simulations of the ARD equation (1).

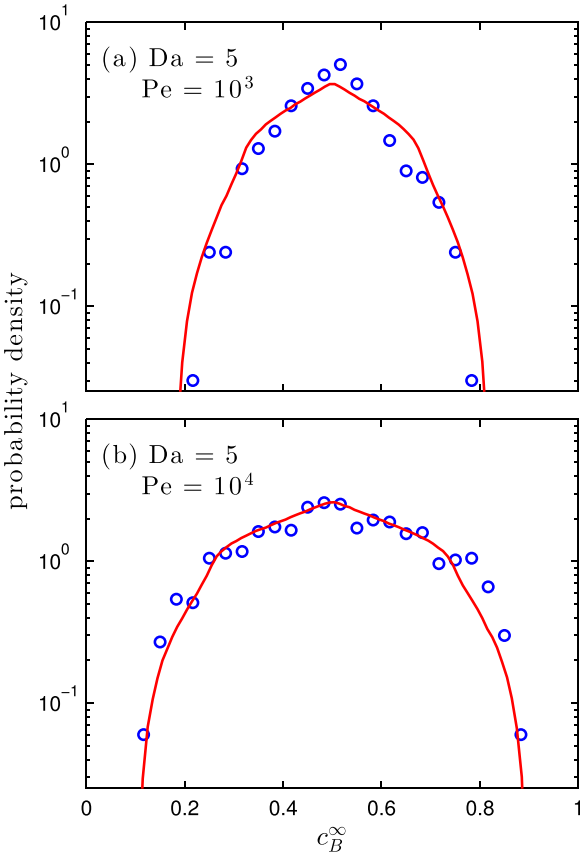

FIG. 9. Probability density functions from simulations (○) and predicted from the FTLE distribution using Eq. (13) (curve) for $\mathrm{Da} = 5$. (a) $\mathrm{Pe} = 10^3$, corresponding to Figures 7(d) and 8(a). (b) $\mathrm{Pe} = 10^4$, corresponding to Figures 7(e) and 8(b).

C. Competitive autocatalytic reaction with recycling

The addition of a recycling reaction to the competitive autocatalytic reactions (R2) is a means to drive the system to a state with only B or C

$$\begin{aligned} A + B &\to 2B, \\ A + C &\to 2C, \\ B + C &\to 2A. \end{aligned} \tag{R3}$$

This is a variation of the recycling reaction studied by Frank,[22] which is $B + C \to 0$. Modifying Eq. (1) slightly to include both the autocatalytic reactions and the recycling reaction yields

$$\frac{\partial c_i}{\partial t} + \boldsymbol{u} \cdot \nabla c_i = \frac{1}{\mathrm{Pe}} \nabla^2 c_i + \mathrm{Da} R_i(c_A, c_B, c_C) + \mathrm{Da}_r R_{r,i}(c_A, c_B, c_C), \tag{14}$$

where $R_{r,i}$ and Da_r are the reaction functions and the Damköhler number associated with the recycling reaction. The initial conditions are the same as those used for competitive autocatalytic reactions in Sec. III B. The reaction functions for the autocatalytic reactions (first two reactions of (R3)) R_i are given in Eq. (10), and the reaction functions for the recycling reaction (last reaction of (R3)) $R_{r,i}$ are

$$\begin{aligned} R_{r,B} &= -c_B c_C, \\ R_{r,C} &= -c_B c_C, \\ R_{r,A} &= 2 c_B c_C. \end{aligned} \tag{15}$$

In Figure 10, the average concentrations of the three species are plotted as functions of time for three different simulations. In Figure 10(a), $L^{(T)} \gg 1$, so B dominates C. C increases in concentration initially, but once most of A has been consumed, B and C react together (3rd reaction in (R3)), consuming most of C in the process, leaving B to eventually occupy the entire domain. The initial bias in concentration generated from the difference in FTLE at the starting location of B and C is amplified to create a final state that contains only B, analogous to results from studies on homochirality.[15] In contrast, Figure 10(b) shows a simulation where $L^{(T)} \approx 1$. In this case, both species stretch similarly early in the flow, so neither species is able to obtain a strong initial bias. This reaction takes much longer to complete than

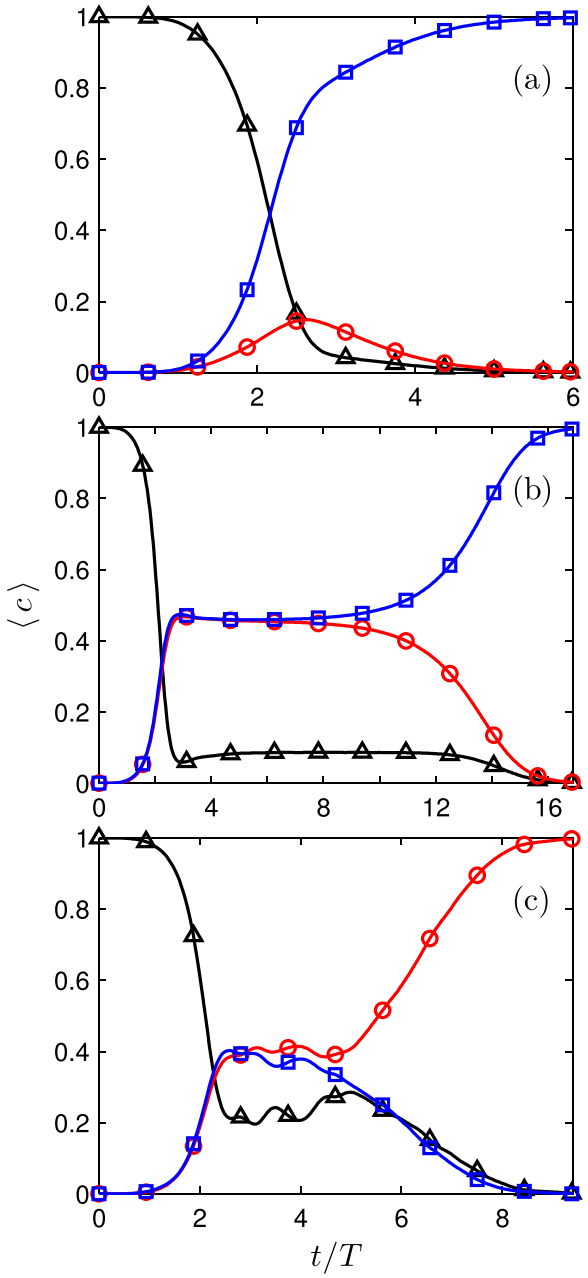

FIG. 10. ARD for an autocatalytic reaction with recycling (R3) under TPSF. Average concentration $\langle c\rangle$ of A (△), B (□), and C (○) as a function of time for $\mathrm{Da}=5$ and $\mathrm{Pe}=10^4$. In (a) and (b), simulations are shown for $\mathrm{Da}_r=1$ for two different initial placements of B and C: (a) $L^{(T)}=689.65/33.61=20.52$, (b) $L^{(T)}=39.72/33.61=1.18$. In (c), $\mathrm{Da}_r=10$, with the same initial placements of B and C as in (b).

the reaction shown in Figure 10(a), as B is unable to quickly overtake C.

In Figure 10(c), the recycling reaction rate is increased (from $\mathrm{Da}_r=1$ to $\mathrm{Da}_r=10$), with the same initial placements of B and C as in panel (b). In this case, C fills the entire domain while B is depleted, showing the sensitivity of the simulation to the recycling reaction rate for $L^{(T)}\approx 1$. Additionally, small oscillations occur in the average concentrations around $t/T\approx 4$, a somewhat counterintuitive result that indicates a competition between the reactions in (R3). Initially, the autocatalytic reactions are prevalent, causing $\langle c_A\rangle$ to decrease. Next, the recycling reaction becomes more prevalent, causing $\langle c_A\rangle$ to increase slightly. The prevalence of the two types of reactions switches back and forth a few times, until eventually $\langle c_A\rangle$ decreases to 0, and only C remains.

Determining which of the two species eventually fills the entire domain depends again on the initial placements of B and C. Whichever species is initially stretched more typically develops a larger average concentration, and this bias is amplified as time progresses.[15,63] Therefore, the species that has a larger FTLE at its starting location should eventually end up filling the entire domain (i.e., if $L^{(\tau)}>1$, B will usually fill the entire domain and $\langle c_B\rangle-\langle c_C\rangle\to 1$, and vice-versa.

To examine this predictive potential, we define $L_*^{(\tau)}=\max(L^{(\tau)},1/L^{(\tau)})$. If $L_*^{(\tau)}\gg 1$, one species will initially be stretched significantly more than the other, and that species should end up filling the entire domain. However, if $L_*^{(\tau)}\approx 1$, both species experience similar degrees of initial stretching, so predicting which species will fill the domain is less certain. To quantify the predictive potential of the FTLE, we define κ to be the probability, over a given range of $L_*^{(\tau)}$, that the species that starts at the higher FTLE fills the entire domain at the end of the simulation. If $\kappa=1$, then

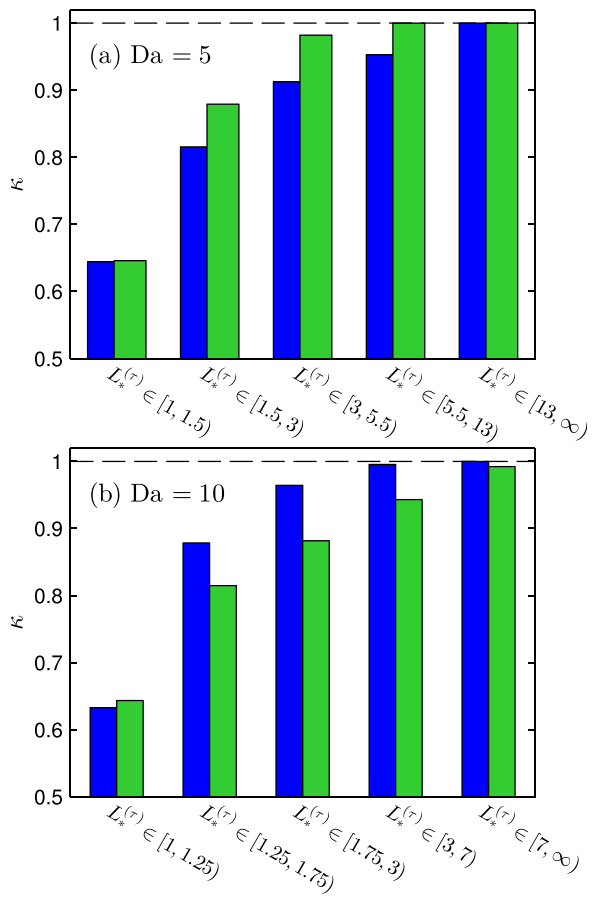

FIG. 11. Bar graphs showing the predictive potential of the FTLE in competitive autocatalytic reactions with recycling for $\mathrm{Pe}=10^3$ (black, blue online) and $\mathrm{Pe}=10^4$ (grey, green online). κ is the probability over a given range of $L_*^{(\tau)}$ that the species that starts at the location with the higher FTLE fills the entire domain. The same values of τ used in Figure 8 are used here: $\tau=T$ for $\mathrm{Da}=5$ and $\tau=T/2$ for $\mathrm{Da}=10$.

the FTLE correctly predicts the species that fills the entire domain for every simulation in the given range of $L_*^{(\tau)}$; if $\kappa = 0.5$, then there is no correlation between the FTLE and which species fills the entire domain. Figure 11 shows the values for κ for different ranges of $L_*^{(\tau)}$ over 1000 simulations at each combination of parameters: $\mathrm{Da} = 5$, 10, $\mathrm{Da}_r = 1$, 2,[64] and $\mathrm{Pe} = 10^3, 10^4$ (8 total different combinations). Results (not shown) indicate that κ does not strongly depend on Da_r in the parameter range studied, so the simulations for $\mathrm{Da}_r = 1$ are combined with the simulations for $\mathrm{Da}_r = 2$ (yielding 4 parameter combinations of interest with 2000 simulations each). The range of $L_*^{(\tau)}$ (abscissa of Figure 11) is chosen such that each bar contains approximately the same number of simulations (approximately 400 per bar). For $L_*^{(\tau)}$ small, κ is close to 0.5, indicating that the FTLE does not accurately predict which species will fill the entire domain. However, as $L_*^{(\tau)}$ increases to larger values (one species starts at a location with a much larger FTLE than the other), κ approaches 1 for all parameter values, indicating that the FTLE approach can always predict which species will fill the entire domain if $L_*^{(\tau)}$ is large enough.

IV. JOURNAL BEARING FLOW

To test the wider applicability of our approach, we consider journal bearing flow, a Stokes flow examined in other ARD studies.[13,20,21] This flow has been extensively studied both computationally and experimentally by Swanson and Ottino,[65] and an analytic solution for the stream function is given by Wannier.[66] Journal bearing flow occurs between two counter rotating cylinders and is shown schematically in Figure 12(a). During each period, the inner cylinder rotates clockwise (at angular speed 2π) for time T_1, and then the outer cylinder rotates counterclockwise (again at angular speed 2π) for time T_2 (so $T = T_1 + T_2$). Here, we use the radius of the inner circle $a_1 = 1/3$, the radius of the outer circle $a_2 = 1$, the eccentricity $e = 0.3$, $T_1 = 2$, and $T_2 = 1$. Figure 12(b) shows streamlines for the individual motions of the outer cylinder rotating and inner cylinder rotating. Streamline crossing indicates that chaos is likely, and the Poincaré section in Figure 12(c) confirms that the velocity field is chaotic throughout most of the domain. The FTLE field for $\tau = T$ is shown in Figure 12(d). In contrast to TPSF which occurs in a periodic domain, journal bearing flow is closed. Additionally, journal bearing flow is not completely chaotic, having regular regions near the edge of both the inner and outer cylinders, as seen in the Poincaré section in

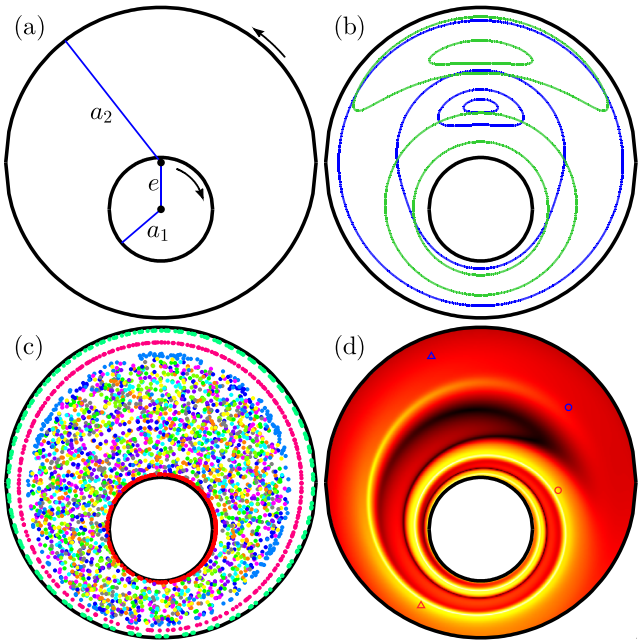

FIG. 12. (a) Schematic of journal bearing flow. During each period, the inner cylinder rotates clockwise at angular speed 2π for time T_1, then the outer cylinder rotates counterclockwise at angular speed 2π for time T_2. Here, we use $a_1 = 1/3$, $a_2 = 1$, and $e = 0.3$. (b) Streamlines for inner cylinder rotating (light grey, green online) and outer cylinder rotating (black, blue online). (c) Poincaré section for $T_1 = 2$ and $T_2 = 1$ for 13 different initial conditions over 300 periods. (d) FTLE field for $\tau = T$, with same colormap as Figure 2 with $\max(\lambda) = 3361$. Starting locations of B and C from Figure 13 are indicated by symbols.

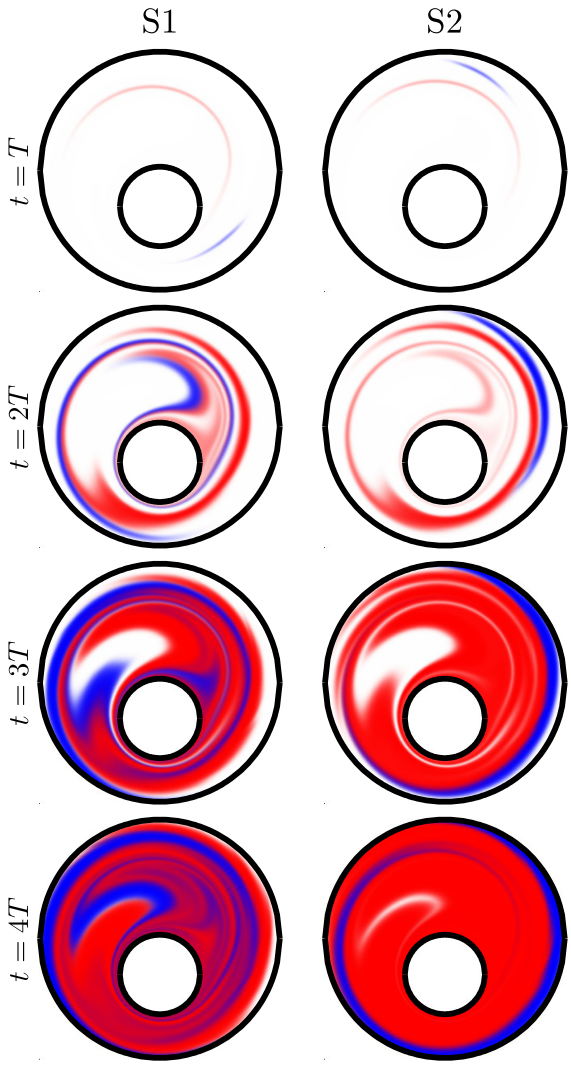

FIG. 13. Concentration distributions of ARD for a competitive autocatalytic reaction without recycling (R2) under journal bearing flow. A (white), B (black, blue online), and C (grey, red online). Initial placements of B and C are shown in Figure 12(d) for S1 (○) and S2 (△). (a) $L^{(T)} = 40.63/1269 = 0.0320$, $c^\infty = 0.335/0.665 = 0.504$. (b) $L^{(T)} = 40.17/1330 = 0.0302$, $c^\infty = 0.167/0.833 = 0.201$. $\mathrm{Da} = 2$, $\mathrm{Pe} = 3 \times 10^4$.

Figure 12(c), while TPSF with $T = 1.6$ is completely chaotic.[67]

Concentration distributions of ARD for a competitive autocatalytic reaction without recycling (R2) under journal bearing flow are shown in Figure 13 for the initial placements shown in Figure 12(d). In simulation S1, $L^{(T)} = 0.032$ and $c^{\infty} = 0.504$, so C occupies about twice as much area as B when the reaction completes. However, in simulation S2, $L^{(T)} = 0.030$, which is similar to $L^{(T)}$ in S1, but now $c^{\infty} = 0.201$, which is much lower than c^{∞} in S1. Based on a similar approach to that used for TPSF, we would expect that similar values for $L^{(T)}$ should give similar values for c^{∞} (see Eq. (12)), which is not the case here. In both S1 and S2, C is initially stretched much more than B, leading to an initial bias for C. However, in S2, B gets trapped near the wall, as evident at $t = 2T$, so B is impeded from spreading further.

"Trapping" of one of the species is a consequence of the closed domain in which journal bearing flow takes place, in contrast to TPSF which takes place in a periodic domain. As a result, a relation like Eq. (12) cannot be expected to describe the dynamics of competitive autocatalytic reactions in closed ARD systems as well as it did for TPSF, as is evident from simulations S1 and S2 in Figure 13. However, the initial stretching of the fluid elements at the starting locations for B and C still plays a significant role, as shown in Figure 14(a), which is a scatter plot of c^{∞} as a function of $L^{(T)}$. There is still a correlation between c^{∞} and $L^{(T)}$, albeit weaker than that for TPSF ($R^2 = 0.84$ in Figure 8(b), and $R^2 = 0.45$ in Figure 14(a)). Additionally, the species that starts at the location with the higher FTLE ends with a higher average concentration in about 77% of the simulations, showing that, despite the somewhat weak correlation in Figure 14(a), FTLEs can potentially play an effective role in predicting the results of the reaction for ARD systems in closed domains.

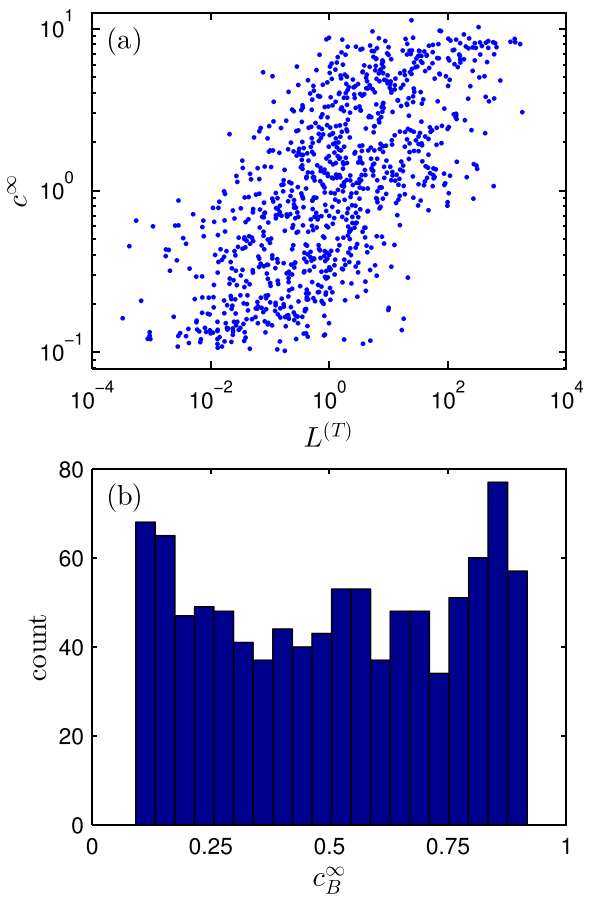

FIG. 14. Results of 1000 simulations of an ARD system undergoing a competitive autocatalytic reaction (R2) for journal bearing flow with $\mathrm{Da} = 2$, $\mathrm{Pe} = 3 \times 10^4$. (a) c^{∞} vs. $L^{(T)}$. (b) Histogram of c_B^{∞}.

Another consequence of "trapping" is that it allows a wider range of values for c_B^{∞}, as can be seen from the histogram in Figure 14(b). This histogram shows that randomly chosen initial placements of B and C result in a distribution of c_B^{∞} values that is roughly uniform. In TPSF, states with c_B^{∞} close to 0 or 1 were unlikely to occur without the addition of recycling. In simulations by Metcalfe and Ottino[21] that also considered journal bearing flow, but from a Lagrangian viewpoint, both states with similar numbers of B and C particles and states with a large disparity in B and C particles were observed, consistent with our results.

V. CONCLUSION

The dynamics of advection-reaction-diffusion systems are important in many applications, and solving these systems accurately and efficiently is an area of ongoing research. In this paper, we presented a numerical method that uses operator splitting and a matrix mapping method to solve the advection-reaction-diffusion equation. This method is computationally efficient and allows for a large number of simulations to be performed in a relatively short time. Hence, statistical approaches can be readily used to study the system under investigation.

Using the operator splitting and matrix mapping method presented in Sec. II B, we simulated the effects of chaotic advection on advection-reaction-diffusion systems for a wide range of the two relevant physical parameters: the Péclet number and the Damköhler number. Small scale stretching that occurs quickly (for times less than one period) often determines the final average concentrations in competitive autocatalytic reactions in ARD systems. A small difference in the FTLE at the starting location of two competing species typically results in approximately equal final concentrations; a large difference yields a state dominated by the species that began at the location with the larger FTLE. Adding a recycling term to the reaction drives the system to a state where only one of the competing species remains, with the FTLE playing a pivotal role in predicting which of the two species fills the entire domain and which is eliminated. The FTLE approach effectively predicts final average concentrations in TPSF, and we expect it to also work well in other chaotic flows that take place in periodic domains. In closed systems such as journal bearing flow, one reactant can become trapped between the other reactant and the system boundary. As a result, the FTLE approach is less reliable in predicting final average concentrations in this instance (compare Figure 8 to Figure 14(a)) but still has significant predictive potential, as we have shown.

A great deal of work remains to be done on this topic. For one, it is not certain that these results, particularly those for the competitive autocatalytic reaction with recycling (R3), will carry over to other flows, including three dimensional flows and other two dimensional flows in both periodic and closed domains. Additionally, we have not yet been able to develop an approach to determine *a priori* τ and γ from Eq. (12). Nevertheless, the use of FTLEs to predict the final average final concentrations in ARD systems appears to have significant potential.

ACKNOWLEDGMENTS

This research was funded by NSF Grant CMMI-1000469.

[1]E. Hernandez-Garcia, C. Lopez, and Z. Neufeld, "Small-scale structure of nonlinearly interacting species advected by chaotic flows," Chaos **12**(2), 470–480 (2002).
[2]Z. Neufeld, "Stirring effects in models of oceanic plankton populations," Chaos **22**(3), 037102 (2012).
[3]S. Edouard, B. Legras, F. Lefevre, and R. Eymard, "The effect of small-scale inhomogeneities on ozone depletion in the arctic," Nature **384**(6608), 444–447 (1996).
[4]J. M. Ottino, "Mixing and chemical-reactions—A tutorial," Chem. Eng. Sci. **49**(24A), 4005–4027 (1994).
[5]T. John and I. Mezic, "Maximizing mixing and alignment of orientable particles for reaction enhancement," Phys. Fluids **19**(12), 123602 (2007).
[6]D. Lima, A. D'Onofrio, and A. De Wit, "Nonlinear fingering dynamics of reaction-diffusion acidity fronts: Self-similar scaling and influence of differential diffusion," J. Chem. Phys. **124**(1), 014509 (2006).
[7]D. Bratsun and A. De Wit, "On marangoni convective patterns driven by an exothermic chemical reaction in two-layer systems," Phys. Fluids **16**(4), 1082–1096 (2004).
[8]M. E. Schwartz and T. H. Solomon, "Chemical reaction fronts in ordered and disordered cellular flows with opposing winds," Phys. Rev. Lett. **100**(2), 028302 (2008).
[9]D. Bargteil and T. Solomon, "Barriers to front propagation in ordered and disordered vortex flows," Chaos **22**(3), 037103 (2012).
[10]J. Mahoney, D. Bargteil, M. Kingsbury, K. Mitchell, and T. Solomon, "Invariant barriers to reactive front propagation in fluid flows," Europhys. Lett. **98**(4), 44005 (2012).
[11]K. A. Mitchell and J. R. Mahoney, "Invariant manifolds and the geometry of front propagation in fluid flows," Chaos **22**(3), 037104 (2012).
[12]T. Buhse, D. Durand, D. Kondepudi, J. Laudadio, and S. Spilker, "Chiral symmetry breaking in crystallization: The role of convection," Phys. Rev. Lett. **84**(19), 4405–4408 (2000).
[13]J. Cartwright, J. Garcia-Ruiz, O. Piro, C. Sainz-Diaz, and I. Tuval, "Chiral symmetry breaking during crystallization: An advection-mediated nonlinear autocatalytic process," Phys. Rev. Lett. **93**(3), 035502 (2004).
[14]D. Kondepudi, R. Kaufman, and N. Singh, "Chiral symmetry-breaking in sodium-chlorate crystallization," Science **250**(4983), 975–976 (1990).
[15]K. Soai, T. Shibata, H. Morioka, and K. Choji, "Asymmetric autocatalysis and amplification of enantiomeric excess of a chiral molecule," Nature **378**(6559), 767–768 (1995).
[16]C. Viedma, "Chiral symmetry breaking during crystallization: Complete chiral purity induced by nonlinear autocatalysis and recycling," Phys. Rev. Lett. **94**(6), 065504 (2005).
[17]W. L. Noorduin, T. Izumi, A. Millemaggi, M. Leeman, H. Meekes, W. J. P. Van Enckevort, R. M. Kellogg, B. Kaptein, E. Vlieg, and D. G. Blackmond, "Emergence of a single solid chiral state from a nearly racemic amino acid derivative," J. Am. Chem. Soc. **130**(4), 1158 (2008).
[18]C. Viedma, J. E. Ortiz, T. de Torres, T. Izumi, and D. G. Blackmond, "Evolution of solid phase homochirality for a proteinogenic amino acid," J. Am. Chem. Soc. **130**(46), 15274 (2008).
[19]S. B. Tsogoeva, S. Wei, M. Freund, and M. Mauksch, "Generation of highly enantioenriched crystalline products in reversible asymmetric reactions with racemic or achiral catalysts," Angew. Chem., Int. Ed. **48**(3), 590–594 (2009).
[20]J. H. E. Cartwright, O. Piro, and I. Tuval, "Ostwald ripening, chiral crystallization, and the common-ancestor effect," Phys. Rev. Lett. **98**(16), 165501 (2007).
[21]G. Metcalfe and J. Ottino, "Autocatalytic processes in mixing flows," Phys. Rev. Lett. **72**(18), 2875–2878 (1994).
[22]F. Frank, "On spontaneous asymmetric synthesis," Biochim. Biophys. Acta **11**(4), 459–463 (1953).
[23]D. Kondepudi and G. Nelson, "Chiral symmetry-breaking in non-equilibrium systems," Phys. Rev. Lett. **50**(14), 1023–1026 (1983).
[24]D. Kondepudi and G. Nelson, "Weak neutral currents and the origin of biomolecular chirality," Nature **314**(6010), 438–441 (1985).
[25]Y. Saito and H. Hyuga, "Complete homochirality induced by nonlinear autocatalysis and recycling," J. Phys. Soc. Jpn. **73**(1), 33–35 (2004).
[26]Y. Saito and H. Hyuga, "Chiral crystal growth under grinding," J. Phys. Soc. Jpn.**77**(11), 113001 (2008).
[27]Y. Saito and H. Hyuga, "Selection of crystal chirality: Equilibrium or non-equilibrium?," J. Phys. Soc. Jpn. **78**(10), 104001 (2009).
[28]Y. Saito and H. Hyuga, "Crystal chirality selected by mutual antagonism," J. Phys. Soc. Jpn. **79**(8), 083002 (2010).
[29]G. Lente, "Homogeneous chiral autocatalysis: A simple, purely stochastic kinetic model," J. Phys. Chem. A **108**(44), 9475–9478 (2004).
[30]Y. Saito, T. Sugimori, and H. Hyuga, "Stochastic approach to enantiomeric excess amplification and chiral symmetry breaking," J. Phys. Soc. Jpn. **76**(4), 044802 (2007).
[31]Y. Saito and H. Hyuga, "Grinding-induced homochirality in crystal growth," J. Cryst. Growth **318**(1), 93–98 (2011), in 16th International Conference on Crystal Growth (ICCG16)/14th International Conference on Vapor Growth and Epitaxy (ICVGE14), Beijing, People's Republic of China, 08–13 August 2010.
[32]F. Muzzio and M. Liu, "Chemical reactions in chaotic flows," Chem. Eng. J. **64**(1), 117–127 (1996).
[33]P. Arratia and J. Gollub, "Predicting the progress of diffusively limited chemical reactions in the presence of chaotic advection," Phys. Rev. Lett. **96**(2), 024501 (2006).
[34]G. Karolyi and T. Tel, "Chemical transients in closed chaotic flows: The role of effective dimensions," Phys. Rev. Lett. **95**(26), 264501 (2005).
[35]Y.-K. Tsang, "Predicting the evolution of fast chemical reactions in chaotic flows," Phys. Rev. E **80**(2), 026305 (2009).
[36]G. Karolyi and T. Tel, "Effective dimensions and chemical reactions in fluid flows," Phys. Rev. E **76**(4), 046315 (2007).
[37]By infinitely fast (or diffusion limited) reactions, we mean that the reaction rate (k) is much larger than a characteristic diffusion rate.
[38]R. Chella and J. M. Ottino, "Conversion and selectivity modification due to mixing in unpremixed reactors," Chem. Eng. Sci. **39**(3), 551–567 (1984).
[39]Z. Toroczkai, G. Karolyi, A. Pentek, T. Tel, and C. Grebogi, "Advection of active particles in open chaotic flows," Phys. Rev. Lett. **80**(3), 500–503 (1998).
[40]G. Karolyi, A. Pentek, Z. Toroczkai, T. Tel, and C. Grebogi, "Chemical or biological activity in open chaotic flows," Phys. Rev. E **59**(5), 5468–5481 (1999).
[41]A. Motter, Y. Lai, and C. Grebogi, "Reactive dynamics of inertial particles in nonhyperbolic chaotic flows," Phys. Rev. E **68**(5), 056307 (2003).
[42]A. de Moura and C. Grebogi, "Reactions in flows with nonhyperbolic dynamics," Phys. Rev. E **70**(3), 036216 (2004).
[43]J. G. Franjione and J. M. Ottino, "Feasibility of numerical tracking of material lines and surfaces in chaotic flows," Phys. Fluids **30**(12), 3641–3643 (1987).
[44]S. Cox, "Chaotic mixing of a competitive-consecutive reaction," Physica D **199**(3–4), 369–386 (2004).
[45]A. Adrover, S. Cerbelli, and M. Giona, "A spectral approach to reaction/diffusion kinetics in chaotic flows," Comput. Chem. Eng. **26**(1), 125–139 (2002).
[46]S. Cerbelli, V. Vitacolonna, A. Adrover, and M. Giona, "Eigenvalue-eigenfunction analysis of infinitely fast reactions and micromixing regimes in regular and chaotic bounded flows," Chem. Eng. Sci. **59**(11), 2125–2144 (2004).
[47]C. P. Schlick, I. C. Christov, P. B. Umbanhowar, J. M. Ottino, and R. M. Lueptow, "A mapping method for distributive mixing with diffusion: Interplay between chaos and diffusion in time-periodic sine flow," Phys. Fluids **25**(5), 052102 (2013).
[48]E. Ott, Y. Du, K. R. Sreenivasan, A. Juneja, and A. K. Suri, "Sign-singular measures: Fast magnetic dynamos, and high-Reynolds-number fluid turbulence," Phys. Rev. Lett. **69**(18), 2654–2657 (1992).

[49]S. W. Jones, "Interaction of chaotic advection and diffusion," Chaos, Solitons Fractals **4**, 929–940 (1994).
[50]I. C. Christov, J. M. Ottino, and R. M. Lueptow, "From streamline jumping to strange eigenmodes: Bridging the lagrangian and eulerian pictures of the kinematics of mixing in granular flows," Phys. Fluids **23**(10), 103302 (2011).
[51]T. Tel, A. de Moura, C. Grebogi, and G. Karolyi, "Chemical and biological activity in open flows: A dynamical system approach," Phys. Rep.-Rev. Sec. Phys. Lett. **413**(2–3), 91–196 (2005).
[52]Y. Saito and H. Hyuga, "Colloquium: Homochirality: Symmetry breaking in systems driven far from equilibrium," Rev. Mod. Phys. **85**(2), 603–621 (2013).
[53]While each species may have a different diffusion coefficient, the analysis is simplified by assuming that all three species have the same diffusion coefficient as this makes the total species concentration the same at all spatial locations. For the competitive autocatalytic reaction scheme (R2), simulations were run where the diffusion coefficient for A was 10 times larger and 10 times smaller than the diffusion coefficient for B and C: the final average concentrations of B and C changed by less than 3%. Thus, it appears that the value for the diffusion coefficient of A has little impact on the results.
[54]J. G. Franjione and J. M. Ottino, "Symmetry concepts for the geometric analysis of mixing flows," Philos. Trans. R. Soc. London, Ser. A **338**(1650), 301–323 1992.
[55]M. Liu, F. J. Muzzio, and R. L. Peskin, "Quantification of mixing in aperiodic flows," Chaos, Solitons Fractals **4**(6), 869–893 (1994).
[56]Z. Neufeld, P. Haynes, and T. Tel, "Chaotic mixing induced transitions in reaction-diffusion systems," Chaos **12**(2), 426–438 (2002).
[57]E. L. Paul, V. A. Atiemo-Obeng, and S. M. Kresta, *Handbook of Industrial Mixing: Science and Practice* (Wiley-Interscience, Hoboken, NJ, 2004).
[58]M. K. Singh, O. S. Galaktionov, H. E. H. Meijer, and P. D. Anderson, "A simplified approach to compute distribution matrices for the mapping method," Comput. Chem. Eng. **33**(8), 1354–1362 (2009).
[59]M. K. Singh, M. F. M. Speetjens, and P. D. Anderson, "Eigenmode analysis of scalar transport in distributive mixing," Phys. Fluids **21**(9), 093601 (2009).
[60]R. Glowinski, "Finite element methods for incompressible viscous flow," in *Handbook of Numerical Analysis, Numerical Methods for Fluids (Part 3)*, edited by P. G. Ciarlet and J. L. Lions (Elsevier, Amsterdam, 2003), Vol. 9.
[61]S. Shadden, F. Lekien, and J. Marsden, "Definition and properties of lagrangian coherent structures from finite-time lyapunov exponents in two-dimensional aperiodic flows," Physica D **212**(3–4), 271–304 (2005).
[62]To calculate c_B^∞ and c_C^∞, the simulation was run to the reaction time t_r for which $\langle c_A(t=t_r)\rangle = 0.001$. From here $c_B^\infty \approx \langle c_B(t=t_r)\rangle/(1-\langle c_A \quad (t=t_r)\rangle) = \langle c_B(t=t_r)\rangle/(0.999)$, and similarly for c_C^∞.
[63]W. Bonner, "The origin and amplification of biomolecular chirality," Orig. Life Evol. Biosph. **21**(2), 59–111 (1991).
[64]The recycling reaction is assumed to be slow ($\mathrm{Da}_r < \mathrm{Da}$), as in Saito and Hyuga (Ref. 25), although similar results are obtained without this assumption.
[65]P. Swanson and J. Ottino, "A comparative computational and experimental-study of chaotic mixing of viscous fluids," J. Fluid Mech. **213**, 227–249 (1990).
[66]G. Wannier, "A contribution fo the hydrodynamics of lubrication," Q. Appl. Math. **8**(1), 1–32 (1950).
[67]In contrast to TPSF, journal bearing flow with these parameters contains visible regular regions. The simulations in this section were also carried out ignoring the regular regions (i.e., B and C were only placed in the chaotic region and the calculation of c_B and c_C only included the chaotic region), and similar results were obtained. This suggests that the presence of a relatively small regular region will not significantly affect the FTLE approach.